Anomalous diffusion in rotating Casson fluid through a porous medium

Liu, Chunyan; Zheng, Liancun; Lin, Ping; Pan, Mingyang; Liu, Fawang

Published in:
Physica A: Statistical Mechanics and its Applications

DOI:
10.1016/j.physa.2019.121431

Publication date:
2019

Anomalous diffusion in rotating Casson fluid through a porous medium

Chunyan Liu[a], Liancun Zheng[a,*], Ping Lin[b], Mingyang Pan[c], Fawang Liu[d]

[a]*School of Mathematics and Physics, University of Science and Technology Beijing, Beijing 100083, China*
[b]*Division of Mathematics, University of Dundee, Dundee DD1 4HN, Scotland, United Kingdom*
[c]*School of Science and Engineering, The Chinese University of Hong Kong, Shenzhen, Shenzhen, Guangdong, 518172, P.R. China*
[d]*School of Mathematical Sciences, Queensland University of Technology, GPO Box 2434, Brisbane, Qld. 4001, Australia*

Abstract

This paper investigates the space-fractional anomalous diffusion in unsteady Casson fluid through a porous medium, based on an uncoupled continuous time random walk. The influences of binary chemical reaction and activation energy between two horizontal rotating parallel plates are taken into account. The governing equations of motion are reduced to a set of nonlinear differential equations by time derivatives discretization and generalized transformation, which are solved by bvp4c and implicit finite difference method (IFDM). Stability and convergence of IFDM are proved and some numerical comparisons to the previous study are presented with excellent agreement. The effects of involved physical parameters such as fractional derivative parameter, rotation parameter and time parameter are presented and analyzed through graphs. Results indicate that the increase of fractional derivative parameter triggers concentration increase near the lower plate, while it causes a reduction near the upper plate. It is worth mentioning that the decrease of heat transfer rate on the plate is seen with the higher time parameter.

Keywords: Casson fluid, Arrhenius reaction, Anomalous diffusion, Implicit finite difference scheme, Stability and convergence

1. Introduction

The convective flow, heat and mass transport in a rotating frame of reference are vital due to their extensive applications such as dynamo effect, food processing, centrifugal filtration, etc. Many studies have been conducted on the modeling of rotating frame motions. The steady and unsteady Couette flows in a rotating frame were considered by Jana et al. [1–3]. Kheshgi and Scriven [4] studied the flow of Newtonian fluid through a rotating square channel. In presence of a magnetic field, Takhar et al. [5] analyzed flow and heat transfer characteristics in a rotating fluid over a stretching surface. They found the skin friction

*Corresponding author.Tel.:+86(10)6233 2589
Email address: liancunzheng@ustb.edu.cn (Liancun Zheng)

coefficient is strongly dependent on the rotation parameter. Later, Sheikholeslami and Ganji [6] discussed the effects of Brownian motion and thermophoresis on nanofluid between two infinite parallel plates with uniform angular velocity. Ghadikolaei et al. [7] explained the influence of magnetic field and volume fraction of carbon nanotubes in a rotating frame. Furthermore, there have been dozens of investigations about this field [8–11].

Diffusion-reaction process with activation energy occurs in applications involving chemical engineering, oil reservoir engineering, food processing, etc. The concentration of reactant plays a key role in the diffusion-reaction process. All kinds of fluids flow under the influence of chemical reaction have been discussed by various researchers. Bestman [12] considered the effect of Arrhenius activation energy on the free convection flow. Further, Makinde et al. [13, 14] examined unsteady convection with Arrhenius reaction and Soret-Dufour effects past a vertical plate. Moreover, Awad et al. [15] investigated the 3D unsteady flow in a rotating viscous fluid with binary chemical reaction and activation energy. The results show the increase in the dimensionless activation energy enhances the concentration profile. In addition, Abbas et al. [16] studied binary chemical reaction on stagnation point flow of Casson fluid. Sajid et al. [17] analyzed Maxwell nanofluid flow with activation energy. However, these models rarely involved Arrhenius activation energy in fractional anomalous diffusion. The appropriate fractional modeling needs to be further considered.

In the past few years, numerous investigations on the anomalous diffusion have been carried out in the complex and heterogeneous background, for instance, porous medium. This interest has been motivated by its importance in some application fields such as hydrology [18], biology [19], electrochemistry [20] and so on. The anomalous diffusion provides super-diffusive or sub-diffusive phenomenon of the transport comparing with the standard diffusion behavior [21–24]. In particular, one way of characterizing this diffusion is the popular continuous time random walk (CTRW) theory [25]. The anomalous super-diffusion is obtained by uncoupled CTRW with the Poissonian waiting time and the Lévy distribution for the jump length [26]. Krepysheva et al. [27] studied the space-fractional advection-diffusion based on CTRW. Pan et al. [28, 29] studied this kind of diffusion problem about space-fractional thermal transfer in nanofluids through a porous medium.

Inspired by the above research, in this paper, we present a study for space-fractional mass transport of Casson fluid in a porous medium, derived from an uncoupled CTRW, in which the influence of Arrhenius reaction in a rotating system is taken into account. The unsteady rotating fluid flow and the heavy-tailed effect of anomalous diffusion are characterized by time parameter t, rotation parameter Ω, and fractional derivative parameter γ, respectively. The structure of the paper is as follows: in Section 2, basic governing equations are proposed. In Section 3, the set of coupled nonlinear equations are solved by using bvp4c and implicit finite difference method (IFDM). Moreover, the stability and convergence of IFDM are proved. The analyses of results and discussion are given in Section 4. Section 5 summarizes the concluding remarks.

2. Basic governing equations

The model consists of flow, heat and space-fractional mass transfer of 3D unsteady Casson fluid between two horizontal parallel plates in a porous medium with Arrhenius reaction condition. The physical model and Cartesian coordinate system used are shown in Fig. 1. The Casson fluid and the plates rotate together around the y-axis with a constant angular velocity Ω. The fixed distance between the upper and lower plates along the y-axis is denoted by h. The x-axis is measured horizontally along the plates, whereas y-axis is taken perpendicular to the plates and normal to the xy-plane is z-axis. To make the position of origin unchanged, the lower plate is stretched linearly with the velocity $u_0 = ax$ $(a > 0)$ by two equal and opposite forces. The rheological model of an isotropic Casson fluid is given by [30]

$$\mathbf{S}_{ij} = \begin{cases} 2(\mu_B + p_y/\sqrt{2\pi})\mathbf{e}_{ij}, & \pi > \pi_c \\ 2(\mu_B + p_y/\sqrt{2\pi_c})\mathbf{e}_{ij}, & \pi < \pi_c \end{cases}, \tag{1}$$

where $\mathbf{e}_{ij}$ is the (i,j)th component of the deformation rate, $\pi = \mathbf{e}_{ij}\mathbf{e}_{ij}$ is the product of the component of the deformation rate with itself, and π_c is a critical value of this product based on the non-Newtonian model. μ_B is the plastic dynamic viscosity of the non-Newtonian fluid and p_y is the yield stress. The reaction rate of binary chemical reaction with Arrhenius activation energy is written as [16]

$$R_C = k_r^2(C - C_h)(T/T_h)^b \exp\left(-E_a/(\kappa T)\right), \tag{2}$$

where k_r^2 is the chemical reaction rate constant. $(T/T_h)^b \exp(-E_a/(\kappa T))$ is the modified Arrhenius function, where κ is the Boltzmann constant and b $(-1 < b < 1)$ is a dimensionless constant. The governing equations of the flow, heat and mass transfer are presented, respectively, as follows:

$$\operatorname{div} \mathbf{V} = 0, \tag{3}$$

$$\rho\left[\frac{\partial \mathbf{V}}{\partial t} + (\mathbf{V}\cdot\nabla)\,\mathbf{V} + 2\Omega \times \mathbf{V} + \Omega \times (\Omega \times \mathbf{r})\right] = -\nabla p + \operatorname{div} \mathbf{S} - \mu \mathbf{V}/\mathrm{K}, \tag{4}$$

$$\frac{\partial T}{\partial t} + (\mathbf{V}\cdot\nabla)T = \alpha \Delta T, \tag{5}$$

$$\frac{\partial C}{\partial t} + (\mathbf{V}\cdot\nabla)C = \tau_1^{\gamma-2} D \cdot \nabla^\gamma C - k_r^2(C - C_h)(T/T_h)^b \exp\left(-E_a/(\kappa T)\right), \tag{6}$$

where $\mathbf{V} = (u, v, w)$ is the velocity components in the direction of Cartesian axes (x, y, z). ρ refers to the fluid density and t is the time. p is the pressure, μ is the dynamic viscosity and K is the permeability of a porous medium. α is the thermal diffusivity and D is the mass diffusivity. The additional coefficient τ_1 is introduced to balance the dimension and we set $\tau_1 = 1$ in the following discussion. $\nabla^\gamma C = D_x^\gamma C + D_y^\gamma C$, where $D_x^\gamma C$, $D_y^\gamma C$ are the fractional Caputo derivatives for $1 < \gamma < 2$ defined by [31]

$$D_x^\gamma C = \frac{\partial^\gamma C}{\partial x^\gamma} = \frac{1}{\Gamma(2-\gamma)} \int_0^x (x - \zeta)^{1-\gamma} \frac{\partial^2 C}{\partial x^2} d\zeta, \tag{7}$$

$$D_y^{\gamma} C = \frac{\partial^{\gamma} C}{\partial y^{\gamma}} = \frac{1}{\Gamma(2-\gamma)} \int_0^y (y-\zeta)^{1-\gamma} \frac{\partial^2 C}{\partial y^2} d\zeta. \tag{8}$$

The Caputo derivative often appears in mass conservation and physical boundary condition, more regular solution profile and zero derivative of constant [32, 33]. The initial and boundary conditions are

$$t \leq 0 : u = v = w = 0, T = T_h, C = C_h \text{ as } y > 0, \tag{9}$$

$$t > 0 : \begin{cases} u = ax, v = w = 0, T = T_0, -D\frac{\partial C}{\partial y} = H_m (C_0 - C) \text{ as } y = 0 \\ u = v = w = 0, T = T_h, C = C_h \text{ as } y = h \end{cases}, \tag{10}$$

where a represents a positive constant, H_m is the convective mass coefficient. To transform Eqs. (3)-(10) in dimensionless forms, we introduce dimensionless units via the transformations

$$\begin{aligned} x^* = \frac{x}{h}, y^* = \frac{y}{h}, z^* = \frac{z}{h}, t^* = \frac{\nu t}{h^2}, u^* = \frac{uh}{\nu}, v^* = \frac{vh}{\nu}, w^* = \frac{wh}{\nu}, \\ \theta^* = \frac{T - T_h}{T_0 - T_h}, \phi^* = \frac{C - C_h}{C_0 - C_h}, p^* = \frac{ph^2}{\rho \nu^2}, \Omega^* = \frac{\Omega h^2}{\nu}, Da = \frac{K}{h^2}. \end{aligned} \tag{11}$$

Substituting (11) into (3)-(10), we obtain the following forms (omitting the superscript $*$ for convenience)

$$\frac{\partial u}{\partial x} + \frac{\partial v}{\partial y} = 0, \tag{12}$$

$$\frac{\partial u}{\partial t} + u\frac{\partial u}{\partial x} + v\frac{\partial u}{\partial y} + 2\Omega w = -\frac{\partial p}{\partial x} + \left(1 + \frac{1}{\beta}\right)\left(\frac{\partial^2}{\partial x^2} + \frac{\partial^2}{\partial y^2}\right) u - \frac{u}{Da}, \tag{13}$$

$$\frac{\partial v}{\partial t} + u\frac{\partial v}{\partial x} + v\frac{\partial v}{\partial y} = -\frac{\partial p}{\partial y} + \left(1 + \frac{1}{\beta}\right)\left(\frac{\partial^2}{\partial x^2} + \frac{\partial^2}{\partial y^2}\right) v - \frac{v}{Da}, \tag{14}$$

$$\frac{\partial w}{\partial t} + u\frac{\partial w}{\partial x} + v\frac{\partial w}{\partial y} - 2\Omega u = \left(1 + \frac{1}{\beta}\right)\left(\frac{\partial^2}{\partial x^2} + \frac{\partial^2}{\partial y^2}\right) w - \frac{w}{Da}, \tag{15}$$

$$\frac{\partial \theta}{\partial t} + u\frac{\partial \theta}{\partial x} + v\frac{\partial \theta}{\partial y} = \frac{1}{\Pr}\left(\frac{\partial^2}{\partial x^2} + \frac{\partial^2}{\partial y^2}\right) \theta, \tag{16}$$

$$\frac{\partial \phi}{\partial t} + u\frac{\partial \phi}{\partial x} + v\frac{\partial \phi}{\partial y} = \frac{1}{Sc}\left(\frac{\partial^{\gamma}}{\partial x^{\gamma}} + \frac{\partial^{\gamma}}{\partial y^{\gamma}}\right) \phi - \sigma (1 + b\delta\theta) e^{-E/(1+\delta\theta)} \phi. \tag{17}$$

The corresponding dimensionless initial and boundary conditions are

$$t \leq 0 : u = v = w = 0, \theta = 0, \phi = 0 \text{ as } y > 0, \tag{18}$$

$$t > 0 : \begin{cases} u = \lambda x, v = w = 0, \theta = 1, \frac{\partial \phi}{\partial y} = -Bi_m (1 - \phi) \text{ as } y = 0 \\ u = v = w = 0, \theta = 0, \phi = 0 \text{ as } y = 1 \end{cases}, \tag{19}$$

where $\beta = \mu_B 2\pi_c / p_y$ is the Casson parameter. Da is the Darcy number, $\sigma = k_r^2 h^2 / \nu$ is the dimensionless chemical reaction rate constant, $\delta = (T_0 - T_h)/T_h$ is the temperature

relative parameter and $E = E_a/(\kappa T_h)$ is the dimensionless activation energy. $\lambda = ah^2/\nu$ is the dimensionless stretching constant, $Pr = \nu/\alpha$ is the Prandtl number, $Sc = \nu/D$ is the Schmidt number and Bi_m is the Biot number of mass diffusion. If the Casson parameter tends to infinite ($\beta \to \infty$), we may regard this model as a Newtonian fluid.

3. Numerical procedure

The FDM solves partial differential equations (PDE)s on a space grid over a series of time steps. For the sake of simplicity, Eqs. (12)-(17) are discretized with a finite difference approximation for the time derivatives, which can be written as

$$\frac{\partial u_n}{\partial x} + \frac{\partial v_n}{\partial y} = 0, \tag{20}$$

$$\frac{u_n - u_{n-1}}{\tau} + u_n\frac{\partial u_n}{\partial x} + v_n\frac{\partial u_n}{\partial y} + 2\Omega w_n = -\frac{\partial p_n}{\partial x} + \left(1+\frac{1}{\beta}\right)\left(\frac{\partial^2}{\partial x^2}+\frac{\partial^2}{\partial y^2}\right)u_n - \frac{u_n}{Da}, \tag{21}$$

$$\frac{v_n - v_{n-1}}{\tau} + u_n\frac{\partial v_n}{\partial x} + v_n\frac{\partial v_n}{\partial y} = -\frac{\partial p_n}{\partial y} + \left(1+\frac{1}{\beta}\right)\left(\frac{\partial^2}{\partial x^2}+\frac{\partial^2}{\partial y^2}\right)v_n - \frac{v_n}{Da}, \tag{22}$$

$$\frac{w_n - w_{n-1}}{\tau} + u_n\frac{\partial w_n}{\partial x} + v_n\frac{\partial w_n}{\partial y} - 2\Omega u_n = \left(1+\frac{1}{\beta}\right)\left(\frac{\partial^2}{\partial x^2}+\frac{\partial^2}{\partial y^2}\right)w_n - \frac{w_n}{Da}, \tag{23}$$

$$\frac{\theta_n - \theta_{n-1}}{\tau} + u_n\frac{\partial \theta_n}{\partial x} + v_n\frac{\partial \theta_n}{\partial y} = \frac{1}{\mathrm{Pr}}\left(\frac{\partial^2}{\partial x^2}+\frac{\partial^2}{\partial y^2}\right)\theta_n, \tag{24}$$

$$\frac{\phi_n - \phi_{n-1}}{\tau} + u_n\frac{\partial \phi_n}{\partial x} + v_n\frac{\partial \phi_n}{\partial y} = \frac{1}{Sc}\left(\frac{\partial^\gamma}{\partial x^\gamma}+\frac{\partial^\gamma}{\partial y^\gamma}\right)\phi_n - \sigma(1+b\delta\theta_n)e^{\frac{-E}{(1+\delta\theta_n)}}\phi_n, \tag{25}$$

where τ is time step, and a truncation error of PDEs is $o(\tau)$. Here u_n, v_n, w_n, θ_n and ϕ_n represent the unknown solutions of nth time level, while u_{n-1}, v_{n-1}, w_{n-1}, θ_{n-1} and ϕ_{n-1} indicate the known quantity of n-1th level ($n = 1, 2, \ldots, N_\tau$). For simplicity of Eqs. (20)-(25) at each time level, we introduce these parameters:

$$u = xf'(\eta), v = -f(\eta), w = xg(\eta), \theta = \theta(\eta), \phi = \phi(\eta), \eta = y. \tag{26}$$

Substituting Eq. (26) into Eqs. (20)-(25) and eliminating the pressure gradient yields the following forms

$$-\tau\left(1+\frac{1}{\beta}\right)f_n^{iv} - \tau f_n f_n''' + \left(1+\frac{\tau}{Da}+\tau f_n'\right)f_n'' + 2\tau\Omega g_n' = f_{n-1}'', \tag{27}$$

$$-\tau\left(1+\frac{1}{\beta}\right)g_n'' - \tau f_n g_n' + \left(1+\frac{\tau}{Da}+\tau f_n'\right)g_n - 2\tau\Omega f_n' = g_{n-1}, \tag{28}$$

$$-\frac{\tau}{\mathrm{Pr}}\theta_n'' - \tau f_n\theta_n' + \theta_n = \theta_{n-1}, \tag{29}$$

$$-\frac{\tau}{Sc}D_\eta^\gamma\phi_n - \tau f_n\phi_n' + \left(1+\tau\sigma(1+b\delta\theta_n)e^{-E/(1+\delta\theta_n)}\right)\phi_n = \phi_{n-1}, \tag{30}$$

with the initial and boundary conditions

$$t \leq 0 : f' = f = g = \theta = \phi = 0 \text{ as } \eta > 0, \tag{31}$$

$$t > 0 : \begin{cases} f' = \lambda, f = g = 0, \theta = 1, \phi' = -Bi_m\,(1-\phi) \text{ as } \eta = 0 \\ f' = f = g = \theta = \phi = 0 \text{ as } \eta = 1 \end{cases}. \tag{32}$$

The primes denote derivative with respect to η.

The physical quantities of engineering interest in flow, heat and mass transfer are the skin friction coefficient C_f, the local Nusselt number Nu_x and the local Sherwood number Sh_x, which are expressed as

$$\begin{gathered} C_f = \frac{\tau_w}{\rho u_0^2} \Longrightarrow Re_x^{-1} C_f = \frac{x}{h^2 \lambda}\left(1 + \frac{1}{\beta}\right) f''(0), \\ Nu_x = \frac{x q_w}{\alpha(T_0 - T_h)} \Longrightarrow Nu_x = -x\theta'(0),\ Sh_x = \frac{x q_m}{D(C_0 - C_h)} \Longrightarrow Sh_x = -x\phi'(0), \end{gathered} \tag{33}$$

where $Re_x = x u_0/\nu$ is the local Reynolds number.

The coupled governing equations (12)-(18), based on time derivatives discretization and generalized transformation, are deduced into a set of nonlinear similarity equations (27)-(31). In order to analyze the influence of involved physical parameters (Da, Ω, Pr, Sc, Bi_m, γ, σ, E, and t), the values of some physical parameters are fixed as: $\tau = 0.01$, $N = 200$, λ=1, b=0.5, β=1.5, and $\delta = 0.5$. In each time level, the solutions of momentum and energy equations of Casson model (27)-(29) are obtained by bvp4c, while the concentration equation (30) is solved by IFDM.

3.1. Solution of momentum and energy problems by bvp4c

In order to check the effectiveness and validity of our numerical schemes, some numerical results verified with previous studies are presented. Where the same boundary conditions and parameters ($R = 1$, $Da = 2$, $\Omega = 0.5$, $\beta \to \infty$ with the conditions of steady-state) are used as in Ref. [6], we validate the algorithm by comparing with the velocity profiles shown in Fig. 2. It is seen from Fig. 2 that the values of velocity generated from the current analysis are in excellent agreement with those from the literature by Sheikholeslami and Ganji [6] for the case of the steady flow of Newtonian fluid.

3.2. Solution of convection anomalous diffusion problem by IFDM

3.2.1. Discretized equation of the convection anomalous diffusion

We define a discrete space point $\eta_j = jh$ and a discrete time point $t_\tau = n\tau$, where $h = 1/N$, $j = 0, 1, \ldots, N$ and $n = 0, 1, \ldots, N_\tau$. Forward difference approximation is utilized for advection term and classical L2 approximation is used to diffusion term [34] in (30). The $\phi_n'(0)$ of the boundary condition (32) is discretized by forward difference approximation of $\phi_n'(0) = (\phi_1^n - \phi_0^n)/h + O(h)$.

The finite difference representation of (30) reads

$$
\begin{aligned}
-\frac{\tau}{Sch^{\gamma}\Gamma(3-\gamma)}\sum_{k=0}^{j-1} d_{j-k}(\phi_{k+2}^{n}-2\phi_{k+1}^{n}+\phi_{k}^{n})-\tau f_j^n\frac{\phi_{j+1}^{n}-\phi_{j}^{n}}{h} \\
+\left(1+\tau\sigma\left(1+b\delta\theta_j^n\right)e^{-E/(1+\delta\theta_j^n)}\right)\phi_j^n=\phi_j^{n-1}
\end{aligned}
\tag{34}
$$

for $j=1,2,\ldots,N-1$ and $n=1,2,\ldots,N_\tau$.

Remark 1. The IFDM of (34) has a local truncation error of e_r=$O(h+\tau)$.

Eqs. (31), (34) and (32) can be expressed in vector-matrix differential equation as follows

$$
A\vec{\phi}^{n}=\vec{\phi}^{n-1}, \tag{35}
$$

where $A=(a_{jk})_{j,k=0}^{N}$ denotes an $(N+1)\times(N+1)$ matrix corresponding to the spatial discretization (31), (34) and (32) at every time step. The 0th row of A is $(1+Bi_m^{-1}h^{-1},-Bi_m^{-1}h^{-1},0,\cdots,0)$ and its Nth row is $(0,0,\cdots,1)$. The components of the jth row of A matrix ($j=1,2,\ldots,N-1$, $k=2,3,\ldots,N$) are

$$
\begin{aligned}
a_{j0}=&\frac{-d_j}{\tau^{-1}Sch^{\gamma}\Gamma(3-\gamma)},\\
a_{j1}=&\frac{-d_{j-1}+2d_j}{\tau^{-1}Sch^{\gamma}\Gamma(3-\gamma)}+\delta_{j1}\left[\frac{\tau f_1^n}{h}+\left(1+\tau\sigma\left(1+b\delta\theta_1^n\right)e^{-E/(1+\delta\theta_1^n)}\right)\right],\\
a_{jk}=&\frac{-d_{j-k}+2d_{j-k+1}-d_{j-k+2}}{\tau^{-1}Sch^{\gamma}\Gamma(3-\gamma)}-\delta_{j,k-1}\frac{\tau f_j^n}{h}\\
&+\delta_{jk}\left[\frac{\tau f_j^n}{h}+\left(1+\tau\sigma\left(1+b\delta\theta_j^n\right)e^{-E/(1+\delta\theta_j^n)}\right)\right],
\end{aligned}
\tag{36}
$$

where $\sigma\left(1+b\delta\theta_j^n\right)e^{-E/(1+\delta\theta_j^n)}>0$ for physical characteristics of the model. δ_{jk} is the Kronecker delta. The non-zero entries of A satisfy the following inequalities [28, 35],

$$
\begin{aligned}
&a_{00}>0, a_{01}<0, a_{N,N-1}=0, a_{NN}=1, a_{jj}>0, \text{ for all } j,\\
&a_{j0}<0 \text{ for } j=1,2,\ldots,N-1, a_{j1}>0 \text{ for } j=2,3,\ldots,N-1,\\
&a_{jk}<0 \text{ for } j=1,2,\ldots,N-1,\ k=2,3,\ldots,j-1,j+1.
\end{aligned}
\tag{37}
$$

3.2.2. Monotonicity of the discretization matrix A

We now prove that A is invertible and $A^{-1}\geq 0$. The off-diagonal entries in column 1 of matrix A are positive, which have a limit on the reversibility of the matrix (see Refs [35, 36]). Then matrix A multiplies by elementary row transformation matrices $E^{(k)}:=(e_{ij}^{(k)})_{i,j=0}^{N}$, where $e_{ij}^{(k)}=\epsilon_{ij}-a_{k0}/a_{00}\cdot\epsilon_{ik}\epsilon_{j0}$. Let $A'=E^{(N-1)}E^{(N-2)}\cdots E^{(1)}A$, and $A'=(a'_{jk})_{j,k=0}^{N}$, where row 0 of A' is $(a_{00},a_{01},0,\cdots,0)$. We clearly obtain

$$
\begin{aligned}
&a'_{j0}=0, \text{ for } j=1,2,\ldots,N-1,\\
&a'_{jk}=a_{jk} \text{ for } k\geq 2 \text{ and all } j,\\
&a'_{11}>0 \text{ and } a'_{j1}<0 \text{ for } j=2,3,\ldots,N-1.
\end{aligned}
\tag{38}
$$

Lemma 3.1. *A' is an M-matrix. Then A is invertible with $A^{-1} \geq 0$, thus the matrix A is monotone.*

Proof. For the matrix A', diagonal entries are positive while off-diagonal entries are non-positive. We have $\sum_{k=0}^{N} a'_{0k} = \sum_{k=0}^{N} a'_{Nk} = 1$. With $\sum_{k=0}^{N} a_{jk} = \left[1+\tau\sigma\left(1+b\delta\theta_j^n\right)e^{-E/(1+\delta\theta_j^n)}\right]$, $(\sigma\left(1+b\delta\theta_j^n\right)e^{-E/(1+\delta\theta_j^n)} > 0)$ for $j = 1, 2, \ldots, N-1$, one has

$$\begin{aligned}\sum_{k=0}^{N} a'_{jk} &= 0 + (a_{j1} + \frac{Bi_m^{-1}h^{-1}}{1+Bi_m^{-1}h^{-1}}a_{j0}) + \sum_{k=2}^{N} a_{jk} \\ &= (\frac{Bi_m^{-1}h^{-1}}{1+Bi_m^{-1}h^{-1}} - 1)a_{j0} + \sum_{k=0}^{N} a_{jk} \\ &= (\frac{Bi_m^{-1}h^{-1}}{1+Bi_m^{-1}h^{-1}} - 1)a_{j0} + \left[1+\tau\sigma\left(1+b\delta\theta_j^n\right)e^{-E/(1+\delta\theta_j^n)}\right] \\ &> 0.\end{aligned} \tag{39}$$

There exists a vector $\vec{w}:=(1,1,\cdots,1)^T$ that satisfies $A'\vec{w} > \vec{0}$. Hence A' is an M-matrix and $(A')^{-1}$ exists with $(A')^{-1} \geq 0$. We can get

$$A^{-1} = (A')^{-1}E^{(N-1)}E^{(N-2)}\cdots E^{(1)}. \tag{40}$$

So A^{-1} exists with $A^{-1} \geq 0$, thus the matrix A is monotone. The proof is completed. □

3.3. Stability and convergence

Lemma 3.2. *A is a monotone matrix of order $N+1$ and there exists a vector $\vec{w}:=(1,1,\cdots,1)^T$ with $\|\vec{w}\|_\infty = 1$ that satisfies $(A\vec{w})_0 = 1$, $(A\vec{w})_N = 1$ and $(A\vec{w})_j = (1+\tau\sigma\left(1+b\delta\theta_j^n\right)e^{-E/(1+\delta\theta_j^n)})$ for $j = 1, 2, \cdots, N-1$. Then $\|A^{-1}\|_\infty \leq 1$ [37].*

Proof. Let $A^{-1} = (\tilde{a}_{jk})_{j,k=0}^{N}$. Since $I = A^{-1}A$ we have for $j = 0, 1, \ldots, N$,

$$1 = \|\vec{w}\|_\infty = \vec{w}_j = (A^{-1}A\vec{w})_j = \sum_{k=0}^{N} \tilde{a}_{jk}(A\vec{w})_k \geq \sum_{k=0}^{N} \tilde{a}_{jk} = (A^{-1}\vec{w})_j, \tag{41}$$

and note that

$$\|A^{-1}\|_\infty = \|A^{-1}\vec{w}\|_\infty, \tag{42}$$

which yields

$$\|A^{-1}\|_\infty = \max_j (A^{-1}\vec{w})_j \leq 1. \tag{43}$$

□

Theorem 3.1. *(stability)*
The IFDM of (34) is unconditionally stable.

Proof. We rewrite (34) as

$$\vec{\phi}^n = A^{-1}\vec{\phi}^{n-1}. \tag{44}$$

Now, we suppose that $\tilde{\phi}^n$ is an approximate solution of (44). The error $\epsilon^n = \tilde{\phi}^n - \vec{\phi}^n$ satisfies

$$\epsilon^n = A^{-1}\varepsilon^{n-1}. \tag{45}$$

By lemma 3.2,

$$\|\epsilon^n\|_\infty = \|A^{-1}\varepsilon^{n-1}\|_\infty \leq \|A^{-1}\|_\infty \|\varepsilon^{n-1}\|_\infty \leq \|\varepsilon^{n-1}\|_\infty. \tag{46}$$

Applying (46) repeatedly n times, we obtain

$$\|\varepsilon^n\|_\infty \leq \|\varepsilon^0\|_\infty. \tag{47}$$

Therefore the IFDM of (34) is unconditionally stable. □

Theorem 3.2. *(convergence)*
The IFDM of (34) is convergent, and the order of convergence is $O(\tau + h)$.

Proof. In order to discuss the convergence of the numerical method, we first give some definitions that $e_j^n = \vec{\phi}(\eta_j, t_n) - \vec{\phi}_j^n$ and $e^n := (e_1^n, e_2^n, \cdots, e_{j-1}^n)^T$. For the initial boundary conditions $e_j^0 = 0$, $e_0^n = 1/(1 + Bi_m h)e_1^n$, $e_N^n = 0$, we can obtain the following error equation

$$e^n = A^{-1}e^{n-1} + M, \tag{48}$$

and $e^0 = 0$, where $M = \tau(O(\tau + h))(1, 1, \cdots, 1)^T$.
Hence we have

$$e^n = ((A^{-1})^n + (A^{-1})^{n-1} + \cdots + (A^{-1})^2 + (A^{-1})^1 + I)M. \tag{49}$$

Then there exists the following inequality

$$\|e^n\|_\infty \leq (\|(A^{-1})^n\|_\infty + \|(A^{-1})^{n-1}\|_\infty + \cdots + \|(A^{-1})^1\|_\infty + \|I\|_\infty)\|M\|_\infty. \tag{50}$$

By lemma 3.2,

$$\|e^n\|_\infty \leq (n+1)\tau|O(\tau + h)|. \tag{51}$$

Consequently, the IFDM of (34) is convergent. □

4. Results and Discussion

In this paper, the unsteady convection flow, heat transfer and space-fractional mass transfer of Casson fluid between two horizontal parallel plates in a porous medium with Arrhenius reaction are studied. The numerical results of velocity, temperature and concentration profiles for different rotation parameter, fractional derivative parameter, time parameter and chemical reaction rate constant are presented and the variations of skin friction coefficient C_f and local Nusselt number Nu_x, as well as local Sherwood number Sh_x are examined.

Fig. 3 shows the influence of different values of the rotation parameter on the velocity distribution in the z-direction. The results in show that as the distance from the lower plate increases, the transverse velocity first increases to the peak value, afterward decreases to 0, meanwhile changes the direction of the velocity to increase again, and then decreases to 0 (reaching the upper plate). The intersection indicates that the transverse velocity is 0, and the velocity on both sides of the intersection increases, but the velocity direction is opposite. It can be seen that intersection moves when the time parameter changes. Moreover, the transverse velocity becomes lower for a bigger value of time parameter ($t = 0.2$) on the lower plate nearby, while the opposite trend close to the upper plate appears. The greater the rotation parameter is, the higher the peaks of transverse velocity distribution curves will be. Besides, with a greater rotation parameter, the transverse velocity of Casson fluid are both faster near the lower plate and the upper plate.

Fig. 4 displays the behavior of fractional derivative parameter γ on the concentration of reactant. The increase of fractional derivative parameter from 1.7 to 2 leads to the enhancement of concentration near the lower plate, while causes a reduction near the upper surface. The intersection shows the tailing phenomenon of anomalous diffusion of reactant concentration in space. Concentration anomalous diffusion in space is delayed compared with normal diffusion, so when the time t and the distance from the lower plate η are fixed, the rate of velocity change of concentration anomalous diffusion is always lower than that of normal diffusion. These results clearly demonstrate that for an increase of fractional derivative parameter, the concentration boundary layer thickness decreases. On the other hand, as shown in Fig. 4, there is the effect of fractional derivative parameter on concentration profile in integer order model with $\gamma = 2$ (the highest order of space derivative) by IFDM, which is compared with the effect of bvp4c. The accuracy of the two algorithms is proved by the height overlap of two lines with $\gamma = 2$.

Fig. 5 illustrates the influence of the fractional derivative parameter on the concentration profile for a fixed position at parameter $\eta = 0.2$. It is seen that the concentration goes up with the increase of time parameter. Moreover, the distribution becomes larger with the increase of fractional derivative parameter at the fixed position t. When the concentration is fixed, the time needed to reach the current concentration is smaller with the increase of the fractional derivative parameter. That is to say, the fractional derivative parameter has the effect of delay and the larger fractional derivative parameter leads to a stronger delay effect.

Fig. 6 shows the distribution curves for parameters $Da = 2, \Omega = 0.5, Pr = 6.2, Sc = 2, Bi_m = 0.9$ and $\gamma = 1.8$ with different values of chemical reaction rate constant σ. It can

be seen from the figure that the concentration of reactant enhances with the increase of time parameter. Meanwhile, the values of concentration in both $E = 0$ and $E = 0.5$ become smaller with the increase of the chemical reaction rate constant. The concentration diffusion curves become lower for a smaller value of dimensionless activation energy E.

Fig. 7 illustrates the behavior of time parameter on concentration field with Casson fluid of high Schmidt number or low Schmidt number. It is observed that concentration increases with the enhancement of time parameter. Also the thickness of concentration boundary layer is noted to thicken with an increment in time parameter. The results indicate, for a larger Schmidt number, the concentration diffusion is slower. In other words, the Schmidt number is smaller and actually the diffusivity for mass transfer is larger, which leads to a decline in concentration. Because the Schmidt number is the ratio of kinematic viscosity and mass diffusivity.

Figs. 8 (*a-c*) show the distribution curves of skin friction coefficient C_f, local Nusselt number Nu_x and local Sherwood number Sh_x. The effects of rotation parameter Ω and Darcy number Da on skin friction coefficient C_f are provided in Fig. 8 (a). It is observed that the skin friction coefficient on the plate increases for higher Darcy number. Physically, the wall friction force rises with augments of permeability of a porous medium. It is important to note that the skin friction coefficient on the smaller rotation parameter is higher than the bigger rotation parameter, when the values of Darcy number are fixed.

Fig. 8 (b) presents the influence of different values of time parameter t and Prandtl number Pr on local Nusselt number Nu_x. It is noticed that with the increasing values of time parameter, the values of local Nusselt number become lower. That is to say, the heat transfer rate significantly decreases for the time. In addition, the local Nusselt number is found to be higher with the increase of Prandtl number at the fixed time parameter. Physically, Prandtl number indicates the ratio of the momentum transfer and thermal diffusion, which affects the thickness of thermal boundary layer. Larger Prandtl number implies weaker thermal diffusivity, which gives a thinner thermal boundary layer and smaller thermal resistance. So the increase of Prandtl number causes the reduction of heat transfer on the surface.

The local Sherwood number Sh_x is plotted as a function of Schmidt number Sc for different Biot number of mass diffusion Bi_m while the other parameters are fixed in Fig. 8 (c). It is clear that the increase of Biot number of mass diffusion enhances the local Sherwood number. Moreover, for larger Schmidt number, the values of the local Sherwood number become stronger. As a result, the mass transfer rate at the plate is physically enhanced with the increase in Schmidt number.

5. Concluding remarks

This paper presents research on unsteady convective flow, heat and space-fractional anomalous diffusion in a rotating Casson fluid between two horizontal parallel plates. We take binary chemical reaction and activation energy in the concentration diffusion model through a porous medium. The numerical solutions of nonlinear equations are obtained by utilizing bvp4c and IFDM. The stability and convergence of IFDM for Eq. (34) are proved. Moreover, the influences of the involved physical parameters on the velocity, temperature

and concentration field are shown graphically and analyzed in detail. We can obtain the following results:

(i) For higher fractional derivative parameter, the reactant concentration increases near the lower plate, while causes a reduction near the upper plate.

(ii) The concentration becomes smaller with the increase of the chemical reaction rate constant.

(iii) The skin friction coefficient is reduced due to the rotation parameter.

(iv) The local Nusselt number decreases as the time parameter rises.

Nomenclature

a	stretching rate
Bi_m	Biot number of mass diffusion
C	concentration
C_f	skin friction coefficient
C_0, T_0	concentration and temperature at lower plate
C_h, T_h	concentration and temperature at upper plate
D	mass diffusivity
Da	Darcy number
E	dimensionless activation energy
g	dimensionless transverse velocity
H_m	convective mass coefficient
K	permeability of the porous medium
k_r^2	chemical reaction rate constant
Nu_x	local Nusselt number
p	pressure
Pr	Prandtl number
q_m	wall mass flux
q_w	wall heat flux
Re_x	local Reynolds number
Sc	Schmidt number
Sh_x	local Sherwood number
t	dimensionless time parameter
u,v,w	velocity in x,y,z-axis direction
u_0	stretching sheet velocity
$\mathbf{V}$	velocity vector
x,y,z	x,y,z-axis
Greek symbols	
α	thermal diffusivity
β	Casson parameter
γ	fractional derivative parameter
η	similarity variable
ϕ	dimensionless variable of C
θ	dimensionless variable of T
μ	dynamic viscosity of fluid
ν	kinematic viscosity
ρ	density of fluid
σ	dimensionless chemical reaction rate constant
τ	dimensionless time step
τ_1	dimensional balance ratio
τ_w	wall shear stress
Ω	rotation parameter

Subscripts	
0	condition at the lower plate
h	condition at the upper plate
Superscript	
$'$	differentiation with respect to η

Acknowledgments

The work of the authors is supported by the National Natural Science Foundations of China (nos. 11772046, 81870345, 11771040, 11861131004).

6. References

[1] R. Jana, N. Datta, Couette flow and heat transfer in a rotating system, Acta Mechanica 26 (1-4) (1977) 301–306.

[2] M. Guria, R. Jana, S. Ghosh, Unsteady Couette flow in a rotating system, International Journal of Non-Linear Mechanics 41 (6-7) (2006) 838–843.

[3] S. Das, S. Maji, M. Guria, R. Jana, Unsteady MHD Couette flow in a rotating system, Mathematical and Computer Modelling 50 (7-8) (2009) 1211–1217.

[4] H. S. Kheshgi, L. Scriven, Viscous flow through a rotating square channel, The Physics of fluids 28 (10) (1985) 2968–2979.

[5] H. S. Takhar, A. J. Chamkha, G. Nath, Flow and heat transfer on a stretching surface in a rotating fluid with a magnetic field, International journal of thermal sciences 42 (1) (2003) 23–31.

[6] M. Sheikholeslami, D. Ganji, Three dimensional heat and mass transfer in a rotating system using nanofluid, Powder Technology 253 (2014) 789–796.

[7] S. Ghadikolaei, K. Hosseinzadeh, M. Hatami, D. Ganji, M. Armin, Investigation for squeezing flow of ethylene glycol (C2H6O2) carbon nanotubes (CNTs) in rotating stretching channel with nonlinear thermal radiation, Journal of Molecular Liquids 263 (2018) 10–21.

[8] T. Hayat, S. Iram, T. Javed, S. Asghar, Shrinking flow of second grade fluid in a rotating frame: an analytic solution, Communications in Nonlinear Science and Numerical Simulation 15 (10) (2010) 2932–2941.

[9] M. A. A. Hamad, I. Pop, Unsteady MHD free convection flow past a vertical permeable flat plate in a rotating frame of reference with constant heat source in a nanofluid, Heat and mass transfer 47 (12) (2011) 1517.

[10] M. Sheikholeslami, D. D. Ganji, M. Y. Javed, R. Ellahi, Effect of thermal radiation on magnetohydrodynamics nanofluid flow and heat transfer by means of two phase model, Journal of Magnetism and Magnetic Materials 374 (2015) 36–43.

[11] M. Hamid, M. Usman, T. Zubair, R. U. Haq, W. Wang, Shape effects of MoS 2 nanoparticles on rotating flow of nanofluid along a stretching surface with variable thermal conductivity: A Galerkin approach, International Journal of Heat and Mass Transfer 124 (2018) 706–714.

[12] A. Bestman, Natural convection boundary layer with suction and mass transfer in a porous medium, International journal of energy research 14 (4) (1990) 389–396.

[13] O. D. Makinde, P. Olanrewaju, W. Charles, Unsteady convection with chemical reaction and radiative heat transfer past a flat porous plate moving through a binary mixture, Afrika Matematika 22 (1) (2011) 65–78.

[14] O. D. Makinde, P. Olanrewaju, Unsteady mixed convection with Soret and Dufour effects past a porous plate moving through a binary mixture of chemically reacting fluid, Chemical Engineering Communications 198 (7) (2011) 920–938.

[15] F. G. Awad, S. Motsa, M. Khumalo, Heat and mass transfer in unsteady rotating fluid flow with binary chemical reaction and activation energy, PloS one 9 (9) (2014) e107622.
[16] Z. Abbas, M. Sheikh, S. Motsa, Numerical solution of binary chemical reaction on stagnation point flow of Casson fluid over a stretching/shrinking sheet with thermal radiation, Energy 95 (2016) 12–20.
[17] T. Sajid, M. Sagheer, S. Hussain, M. Bilal, Darcy-Forchheimer flow of Maxwell nanofluid flow with nonlinear thermal radiation and activation energy, AIP Advances 8 (3) (2018) 035102.
[18] F. Liu, I. Turner, V. Anh, An unstructured mesh finite volume method for modelling saltwater intrusion into coastal aquifers, Journal of Applied Mathematics and Computing 9 (2) (2002) 391–407.
[19] P. Perdikaris, G. E. Karniadakis, Fractional-order viscoelasticity in one-dimensional blood flow models, Annals of biomedical engineering 42 (5) (2014) 1012–1023.
[20] A. Ehsani, M. Mahjani, M. Bordbar, S. Adeli, Electrochemical study of anomalous diffusion and fractal dimension in poly ortho aminophenol electroactive film: Comparative study, Journal of Electroanalytical Chemistry 710 (2013) 29–35.
[21] H. Qi, X. Jiang, Solutions of the space-time fractional Cattaneo diffusion equation, Physica A: Statistical Mechanics and its Applications 390 (11) (2011) 1876–1883.
[22] B. Yu, X. Jiang, H. Xu, A novel compact numerical method for solving the two-dimensional non-linear fractional reaction-subdiffusion equation, Numerical Algorithms 68 (4) (2015) 923–950.
[23] A. A. Zhokh, A. I. Trypolskyi, P. E. Strizhak, An investigation of anomalous time-fractional diffusion of isopropyl alcohol in mesoporous silica, International Journal of Heat & Mass Transfer 104 (2017) 493–502.
[24] H. Zhang, X. Jiang, X. Yang, A time-space spectral method for the time-space fractional fokker–planck equation and its inverse problem, Applied Mathematics and Computation 320 (2018) 302–318.
[25] A. P. Pereira, J. Fernandes, A. Atman, J. Acebal, Parameter calibration between models and simulations: Connecting linear and non-linear descriptions of anomalous diffusion, Physica A: Statistical Mechanics and its Applications.
[26] R. Metzler, J. Klafter, The random walk's guide to anomalous diffusion: a fractional dynamics approach, Physics reports 339 (1) (2000) 1–77.
[27] N. Krepysheva, L. Di Pietro, M.-C. Néel, Space-fractional advection-diffusion and reflective boundary condition, Physical Review E 73 (2) (2006) 021104.
[28] M. Pan, L. Zheng, F. Liu, X. Zhang, Modeling heat transport in nanofluids with stagnation point flow using fractional calculus, Applied Mathematical Modelling 40 (21) (2016) 8974–8984.
[29] M. Pan, L. Zheng, F. Liu, C. Liu, X. Chen, A spatial-fractional thermal transport model for nanofluid in porous media, Applied Mathematical Modelling 53 (2018) 622–634.
[30] D. Pal, N. Roy, K. Vajravelu, Effects of thermal radiation and Ohmic dissipation on MHD Casson nanofluid flow over a vertical non-linear stretching surface using scaling group transformation, International Journal of Mechanical Sciences 114 (2016) 257–267.
[31] A. Saadatmandi, M. Dehghan, A tau approach for solution of the space fractional diffusion equation, Computers & Mathematics with Applications 62 (3) (2011) 1135–1142.
[32] X. Zhang, M. Lv, J. W. Crawford, I. M. Young, The impact of boundary on the fractional advection–dispersion equation for solute transport in soil: Defining the fractional dispersive flux with the caputo derivatives, Advances in Water Resources 30 (5) (2007) 1205–1217.
[33] R. K. Pandey, O. P. Singh, V. K. Baranwal, An analytic algorithm for the space–time fractional advection–dispersion equation, Computer Physics Communications 182 (5) (2011) 1134–1144.
[34] S. Shen, F. Liu, Error Analysis of an Explicit Finite Difference Approximation for the Space Fractional Diffusion Equation with Insulated Ends, Anziam Journal 46 (2005) 871–887.
[35] M. Stynes, J. L. Gracia, A finite difference method for a two-point boundary value problem with a Caputo fractional derivative, IMA Journal of Numerical Analysis 35 (2) (2015) 698–721.
[36] J. L. Gracia, M. Stynes, Central difference approximation of convection in Caputo fractional derivative two-point boundary value problems, Journal of Computational and Applied Mathematics 273 (2015) 103–115.
[37] O. Axelsson, L. Kolotilina, Monotonicity and discretization error estimates, Society for Industrial and

Applied Mathematics, 1990.

Figures

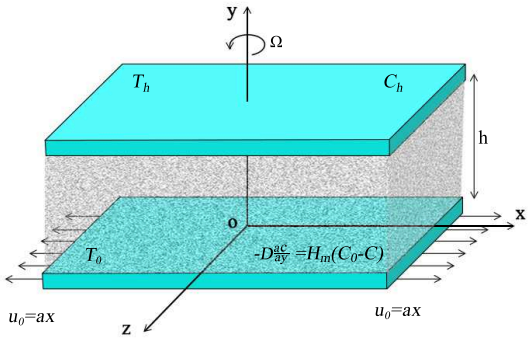

Fig. 1: Schematic of the physical model under study.

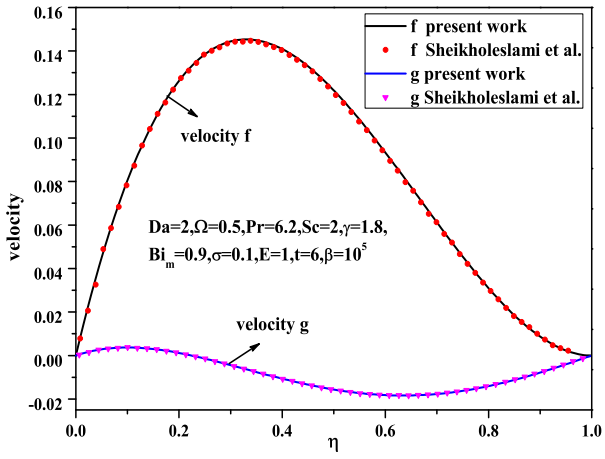

Fig. 2: The comparison of velocity profiles between the present work and Sheikholeslami and Ganji [6] at $R = 1$ when $Da = 2$, $\Omega = 0.5$, $\beta \to \infty$ with the conditions of steady-state.

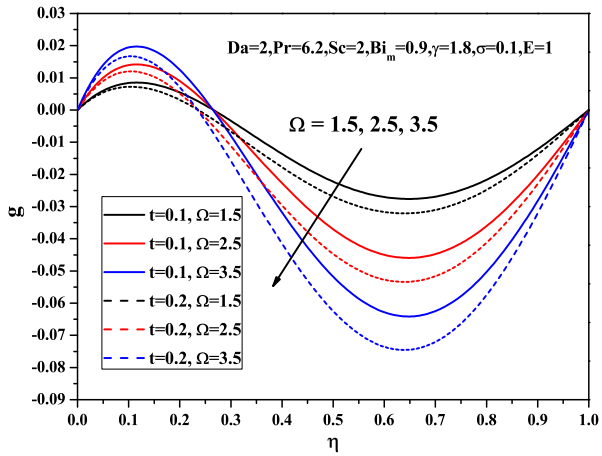

Fig. 3: Transverse velocity g for different values of the rotation parameter Ω.

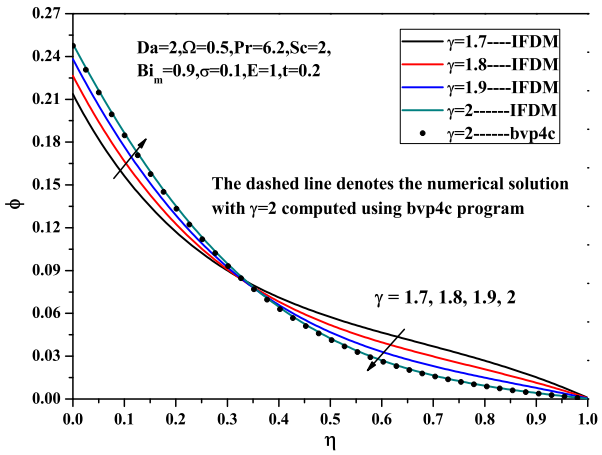

Fig. 4: Concentration ϕ for different values of the fractional derivative parameter γ.

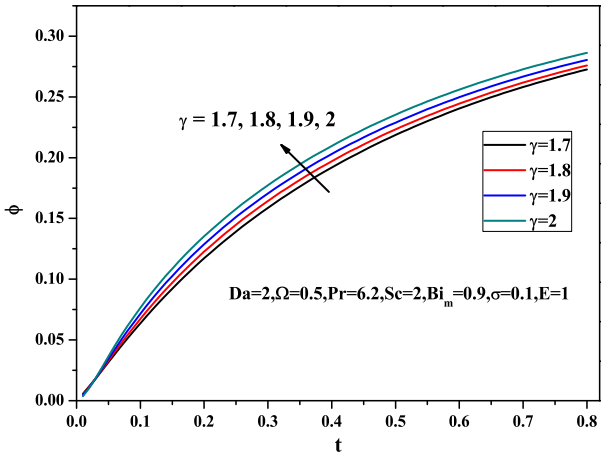

Fig. 5: Concentration ϕ for different values of the fractional derivative parameter γ at $\eta = 0.2$.

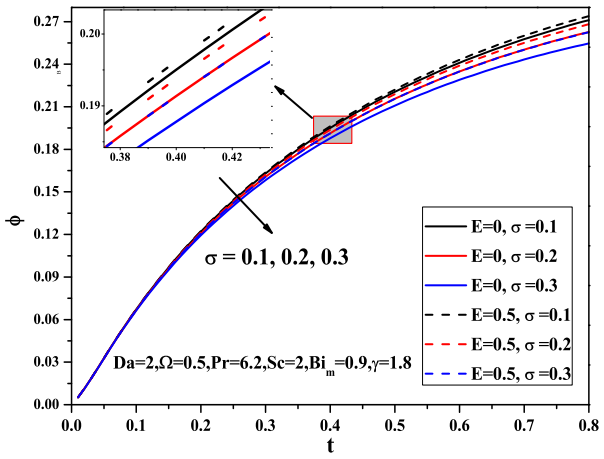

Fig. 6: Concentration ϕ for different values of the chemical reaction rate constant σ at $\eta = 0.2$.

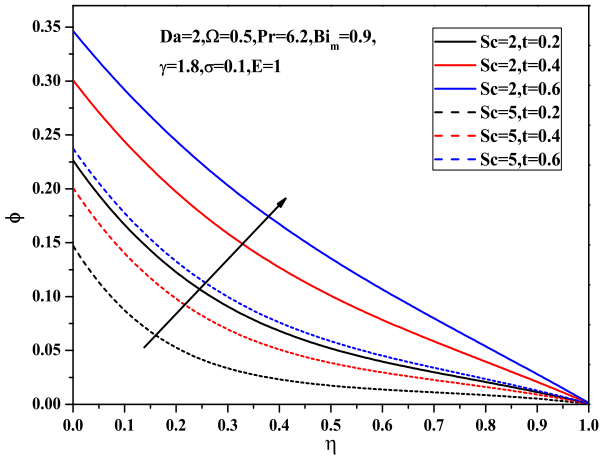

Fig. 7: Concentration ϕ for different values of the time parameter t.

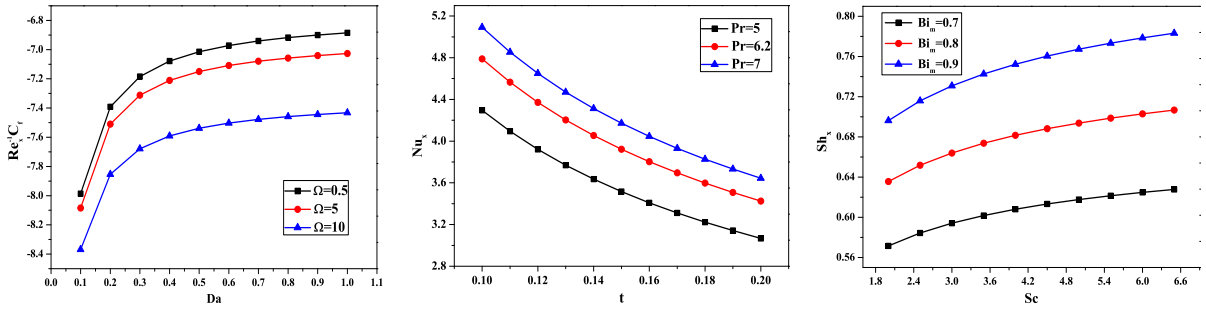

(a) Effects of Ω on C_f (b) Effects of Pr on Nu_x (c) Effects of Bi_m on Sh_x

Fig. 8: Physical quantities at the wall: skin friction coefficient, local Nusselt number and local Sherwood number.